Wind and Structures, Vol. 5, No. 2~4 (2002) 347-358
DOI: http://dx.doi.org/10.12989/was.2002.5.2_4.347

Comparison of numerical and wind tunnel simulation of wind loads on smooth, rough and dual domes immersed in a boundary layer

R. N. Meroney†

Civil Engineering Department, Colorado State University, Fort Collins, CO 80523, USA

C. W. Letchford† and P. P. Sarkar‡

Wind Science and Engineering Research Center, Texas Tech University, Lubbock TX 79409, USA

Abstract. Mean surface pressures and overall wind loads on hemispherical domes immersed in a boundary layer were obtained by numerical simulation. The effects of alternative turbulence models, Reynolds Number and surface roughness were examined and compared with earlier studies. Surface pressures on dual hemispherical domes were also calculated for three wind orientations (0^o, 45^o, and 90^o) to evaluate flow field interactions. Calculated values were compared to wind-tunnel measurements made in equivalent flow conditions.

Key words: wind loads; computational wind engineering; fluid modeling; hemispherical domes.

1. Introduction

Domed roofs have always fascinated architects not only because of their graceful curves, but because they provide wide unsupported interior spaces. Membrane structures for long-span and lightweight roofs can be incorporated into spherical pneumatic domes. Such air-supported structures are usually made from relatively thin, flexible but impervious materials that are sometimes reinforced by or supported by cables. Although domes are excellent at resisting symmetric loading, the structures are sensitive to asymmetric loading that may cause failure or loss of cladding. Air pressures within inflated structures must be sufficient to prevent buckling and collapse in high winds, but not so large that the membrane is torn by the large tensions that may develop (Newman and Ganguli 1984).

Many wind tunnel studies have been undertaken to determine wind loads on domes and hemispheres in boundary layer flows. Early work by Maher (1965) was in uniform flow with little approach flow turbulence. Other authors included a turbulent shear flow over a range of Reynolds numbers (Taniguchi & Sakamato 1981, Tou *et al*. 1983, Newman *et al*. 1984, Savoy & Toy 1986), but only Ogawa *et al.* (1991), Taylor (1991) and Letchford and Sarkar (2000) presented

† Professor
‡ Associate Professor

measurements of fluctuating pressures. Letchford and Sarkar provided dual dome mean, rms and peak pressure contours and loads.

An additional complication associated with both wind tunnel and numerical studies for these types of structures is due to the curved surface, which leads to Reynolds Number effects. Local boundary layers growing on the dome surface will determine whether flow separation and reattachment will occur along the dome exterior. In turn recirculating flows associated with such separation determine the shape and magnitude of pressures over a large portion of the domed surface. Since the separation locations cannot be identified or specified purely based on geometry, this has led to large uncertainties when measuring or calculating pressure loads. Taylor concluded during his wind tunnel measurement program that as long as the Reynolds Numbers exceeds 2×10^5 and turbulence intensity exceeds 4% the surface pressure distributions are largely independent of Reynolds Number, but this has not been confirmed for multiple dome situations. Computational boundary layers are also sensitive to selection of wall functions, turbulence models and inlet flow conditions.

The present study uses Computational Fluid Dynamic (CFD) methods to examine wind loading on single and paired sets of domes and to compare the effects of turbulent model selected, Reynolds number and surface roughness with previous wind-tunnel studies. A commercial code suite produced by FLUENT © Inc. was used to perform the calculations rather than codes created to be application specific to determine whether software in the public domain would suffice to produce results suitable for design purposes.

2. Dome geometry and wind tunnel configuration

The prototype dome dimensions selected for study have an approximate sphere diameter of 168 m, but were truncated to a base diameter of 144 m and a height (h) of 45 m. At a scale of 1:300 fiberglass models of parabolic domes of nearly spherical shape, base diameter of 480 mm and apex height of 150 mm were studied in the Industrial Wind Tunnel at Colorado State University by Letchford and Sarkar (2000). When two domes were studied together they were separated at the base by 100 mm (30 m at full scale). The models were covered with “gel coat” to obtain a very smooth surface. To obtain a rougher surface the models were covered with a tailored fly screen mesh of 0.3 mm diameter fiber at 1.5 mm spacing. One dome was instrumented with 85-pressure taps spread along 12 meridians at 30^o increments.

The wind tunnel created a simulation of Exposure C, ASCE7-98 wind code conditions at a scale of 1:300 by using 4 upwind spires, a 240 mm fence and 18 mm chain floor roughness at 200 mm spacing up to the model domes. The mean velocity and turbulence intensity at model apex height were 18 m/s and 15%, respectively. Test Reynolds Number was approximately 4.6×10^5. These boundary layer characteristics were also the target values for inlet conditions to the test domain for the numerical calculations.

Letchford and Sarkar (2000) describe further details of the wind-tunnel procedures. Mean pressures were obtained from 96-second records of pressures using instrumentation with frequency response flat to 160 Hz. This suggests equivalent full-scale mean values that were averaged over periods exceeding 1 hour from instrumentation with a frequency response of 1.6 Hz. All pressures were non-dimensionalized into pressure coefficient by dividing by a reference dynamic pressure at the top of the dome [i.e., $Cp = \Delta p / (1/2\ \rho U^2)$]

3. Numerical procedure

Flow and dispersion over various building pattern arrangements were simulated with the FLUENT© suite of computational fluid dynamics software. This software is based on a finite volume discretization of the equations of motion, an unstructured grid volume made of either rectangular prisms or tetrahedral cells, various matrix inverting routines, and, in this case, either kappa-epsilon (κ-ε), Reynolds stress (RMS) or Spalart-Allmaras (SA) turbulence models (See Wilcox 1993, Spalart and Allmaras 1992). The standard κ-ε and the Reynolds-stress models required the use of wall functions. Steady state solutions were sought for several flow configurations, and the data generated were displayed on various isopleth contour plots of velocity, pressure, and turbulence. Particle trajectories were also generated to elucidate the effects of dome spacing. The code was run on a Pentium Pro 400 MHz PC using a Microsoft NT 4.0 operating system.

3.1. Inlet conditions to the numerical domain

Version 5.3.18 of the FLUENT code was used for all numerical simulations. Equilibrium inlet profiles were prepared computationally by calculating outflow profiles through a long duct of equivalent cross-section, length, spire configurations, barriers and surface roughness. This separate numerical wind tunnel and grid were used to preprocess inlet conditions to assure that inlet mean velocity, turbulent kinetic energy and dissipation profiles were similar to those measured in the wind tunnel and in dynamic equilibrium with one another. The numerical grid used in the inlet condition preprocessor step is shown in Fig. 1. The inlet mean velocity and turbulence intensity profiles used are shown in Figs. 2a and 2b, respectively, and compared with wind tunnel measurements and ASCE7-98 target values. The ground surface roughness measured during the laboratory experiments was 1.7×10^{-4} m or an equaivalent sand roughness, k, equal to 5 mm. Values deduced from the numerical wind tunnel for these parameters were 2.3×10^{-4} m and 7 mm, respectively. All velocity profiles are essentially collinear, and the numerical and wind tunnel turbulence intensity values are also very similar.

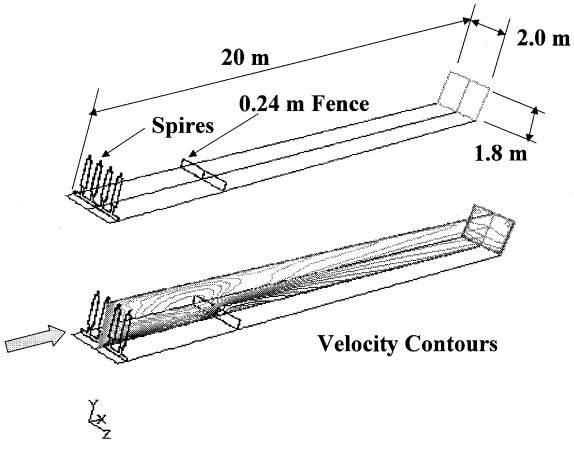

Fig. 1 Numerical wind-tunnel grid for calculating inlet profiles. Grid includes upwind spires, fence and surface roughness. Domain is 2 m × 2 m × 20 m long

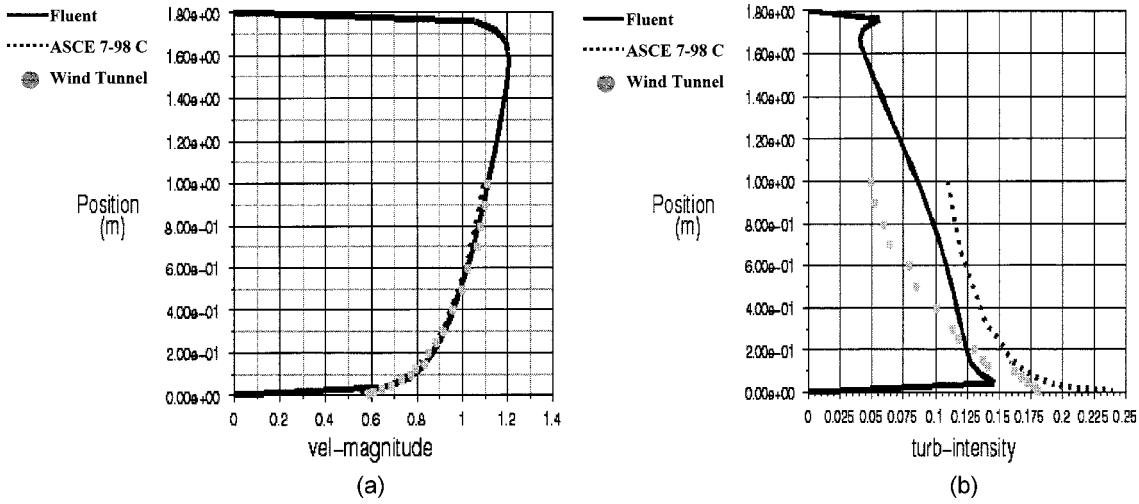

Fig. 2 (a) Numerical inlet velocity profile compared to wind-tunnel measurements and target ASCE-98 C code profiles. (b) Numerical inlet turbulent intensity profile compared to wind-tunnel measurements and target ASCE-98 C code profiles

3.2. Numerical domain

Various calculation domains were chosen, depending on the number of domes and the wind orientation. The typical numerical domain represented a 2 m wide wind tunnel, 2 m flow depth, and a 4 m test section length. The example single dome configuration shown in Fig. 3 contained some 16371 cells, 51,733 faces and 19,105 nodes distributed over 13 face zones. Outlet and velocity inlet or symmetry boundaries were specified at the sides and top of the grid volume, while appropriate surface roughness was specified at the ground. As noted in Section 3.1, the inflow boundary conditions were chosen to match the velocity and turbulence profiles measured during the wind-

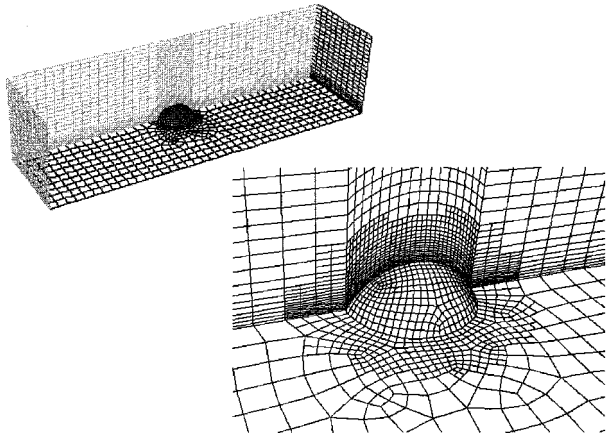

Fig. 3 Rectangular domain and grid for single hemispherical dome using octagonal grid elements and a graded boundary layer near the floor. Domain is 1 m × 2 m × 4 m long

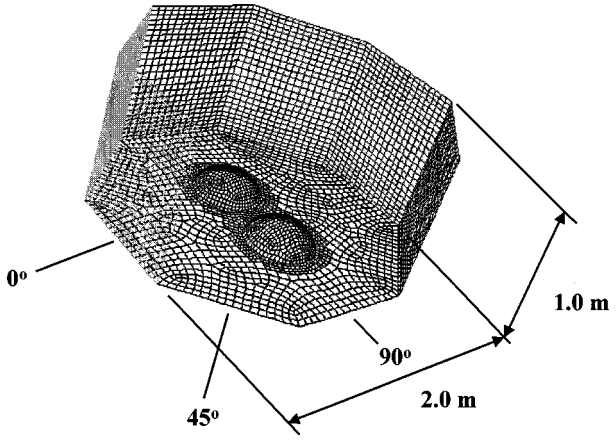

Fig. 4 Octagonal domain and grid for dual hemispherical domes using tetrahedral grid elements and a graded boundary layer near the floor. Domain is 2 m × 2 m × 2 m long

tunnel experiments. Outflow boundary conditions were chosen to maintain constant longitudinal rate of change of all dependent variables (i.e., constant slope).

Both rectangular and octagonal calculation domains were used to calculate flows over the dome pairs. For the 0^o and 90^o wind orientations rectangular domains were studied, but a unique octagonal domain was created to permit studying 0^o, 45^o and 90^o wind orientations without creating separate (and possibly different) grid arrangements. These grids contained some 43,004 cells, 133,577 faces and 47,697 nodes distributed over 14 face zones. Simply by selecting the specification for side boundaries from inlet, sidewall, and outlet designations different orientations could be specified.

Fig. 4 displays one of the different grid orientations studied.

4. Numerical results

4.1. Single dome flow and pressure behavior

Flow approaching the single dome decelerates along the centerline, stagnates against the surface and produces a maximum mean pressure coefficient stagnation region of about $Cp = 0.5–0.6$ at a height of $y / h = 0.2$. An extremely weak horseshoe shaped vortex forms on the front face and wraps around the dome downwind. The flow accelerates over the dome apex producing a minimum mean pressure coefficient region of about $Cp = –0.8–0.9$ that lies acorss the top of the dome. The flow decelerates again as it descends over the back of the dome, and the pressure coefficient reaches positive values over the very end of the dome down to the ground. At most a very weak recirculation cavity exists at the dome downwind face. Greater grid resolution in this region might identify the flow more accurately. Fig. 5 displays contour plots of mean pressure coefficient as observed from above and to the side.

Fig. 6 compares the mean centerline pressure coefficient distribution plotted versus profected stream wise direction on the smooth dome with that measured by Letchford and Sarkar (2000) and by Taylor (1991) for a true spherical dome $h / D = 1/3$ at a similar Reynolds Number and turbulence intensity. Both the numerical calculations and the Letchford and Sarkar data display positive

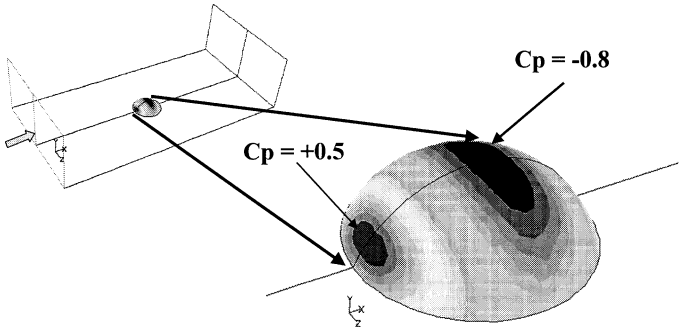

Fig. 5 Contour isopleths of mean pressure coefficient over the hemispherical dome for numerically calculated case for a rectangular domain and hexagonal grid elements

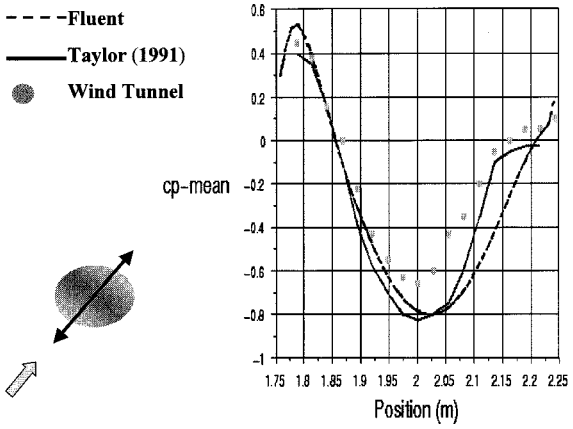

Fig. 6 Centerline mean pressure coefficient profile over a single hemispherical dome compared to wind-tunnel measurements of Letchford and Sarkar (2000) and Taylor (1991)

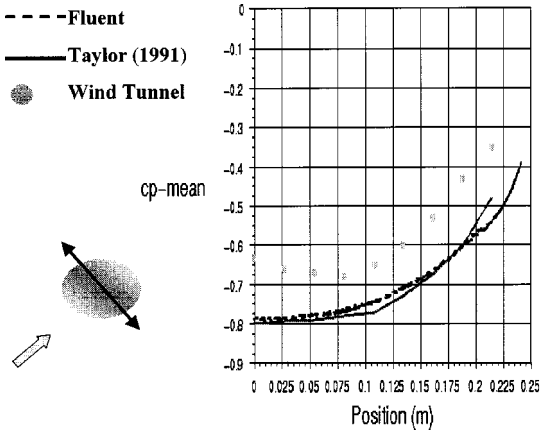

Fig. 7 Meridian mean pressure coefficient profile over a single hemispherical dome compared to wind-tunnel measurements of Letchford and Sarkar (2000) and Taylor (1991)

pressure coefficients over the downwind face of the dome. Fig. 7 makes the same comparison for the 90° meridian. The distributions are very similar in shape agreeing with both measurement sets on the windward side of the dome, but tending to follow Taylor's results more closely over the top and downwind side of the dome. Along the meridian lines computed profiles agree most closely with the Taylor data.

Numerical calculations of mean pressure coefficient distributions at Reynolds numbers of 185,000 and 1,440,000 were essentially equivalent, indicating any separation and reattachment patterns were similar. Calculations were also performed using the κ-ε two-equation, the Reynolds stress seven-equation, and the Spalart-Allmaras one-Allmaras one-equation turbulence models. Pressure distributions were essentially equivalent with only small relative perturbations. This was rather surprising given the propensity for the standard κ-ε model to over-predict turbulent energies in shear regions around bluff bodies resulting in under-prediction or elimination of some separation regions. But the wind-tunnel experiments also exhibited very minor separation in the wake, perhaps because the shapes are curved and immersed in a turbulent shear layer.

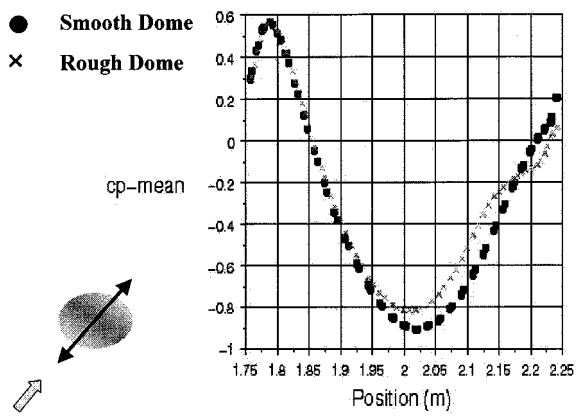

Fig. 8 Centerline mean pressure coefficient profile over single smooth and single rough domes

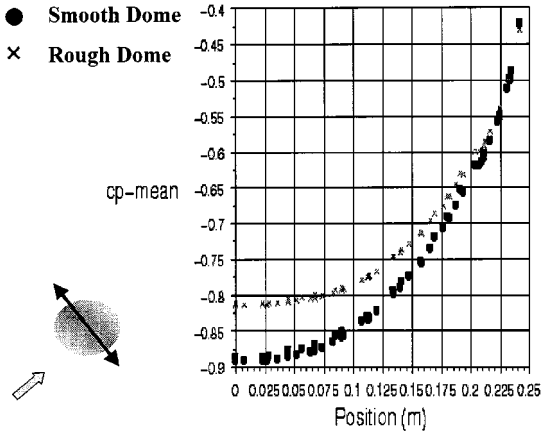

Fig. 9 Meridian mean pressure coefficient profile over single smooth and single rough domes

Figs. 8 and 9 show similar comparisons between mean pressure coefficients for the smooth and rough domes. The roughness is seen to reduce the suction over the surface of the domes and decrease the magnitude and extent of the positive pressure coefficient over the downwind side of the dome. The wind-tunnel measurements performed by Letchford and Sarkar showed similar effects of surface roughness; however, magnitudes differed from numerical results in a similar manner to that shown in Figs. 6 and 7.

4.2. Dual dome flow and pressure behavior

Flow and pressure behavior were calculated for the dual domes oriented at approach wind angles of 0^o, 45^o and 90^o, where a 0^o orientation places the domes at maximum wind exposure and 90^o orientation places the domes in a tandem arrangement with one behind the other.

4.2.1. Zero degree orientation case

During the 0^o flow conditions stagnation regions, apex suctions and wake pressures are almost identical on the two domes. However, flow appears to accelerate somewhat in the gap between the two domes, resulting in asymmetric meridian pressure profiles with lower pressures in the gap region. Fig. 10 compares mean pressure contours measured over dual domes by Letchford and Sarkar with those calculated by the Fluent programs. Figs. 11 and 12 compare centerline and meridian pressure profiles.

4.2.2. Forty-five degree orientation case

During the 45^o flow conditions centerline winds are diverted to the side through the gap between the domes. Fig. 13 displays path line trajectories from horizontal and vertical tracer rakes placed upwind of the domes. Pressure contours look similar, but stagnation pressures are somewhat higher and suction pressures somewhat lower on the upwind dome. That is for the upwind and downwind

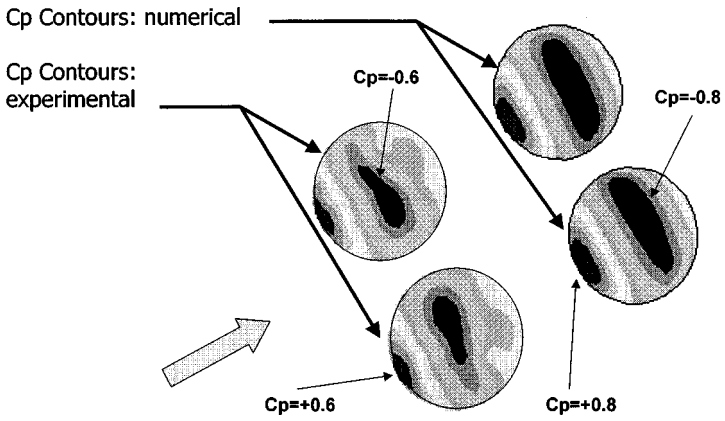

Fig. 10 Contour isopleths of mean pressure coefficient over dual hemispherical domes for wind-tunnel measurements of Letchford and Sarkar (2000) and numerically calculated cases for an octagonal domain and tetrahedral grid elements : 0° approach angle

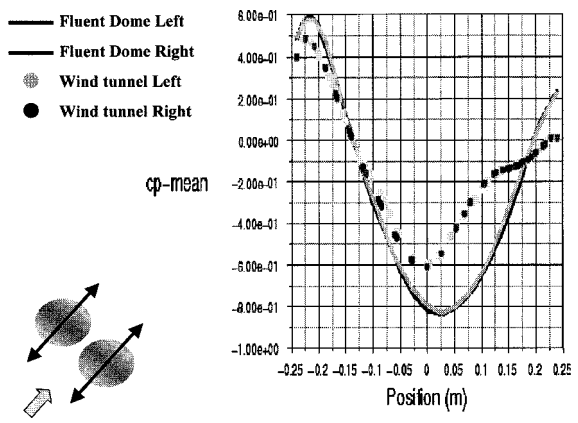

Fig. 11 Centerline mean pressure coefficient profiles over dual hemispherical domes compared to wind-tunnel measurements of Letchford and Sarkar (2000) : 0° approach angle

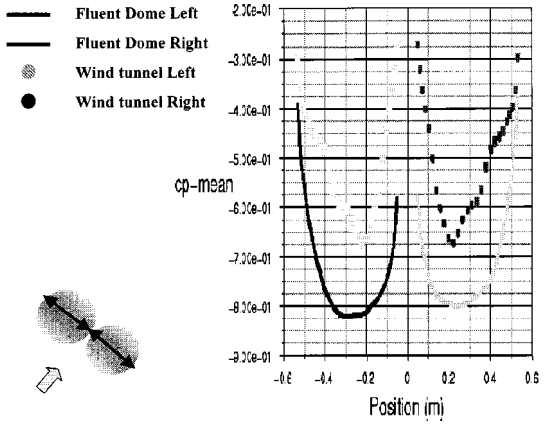

Fig. 12 Meridian mean pressure coefficient profiles over dual hemispherical domes compared to wind-tunnel measurements of Letchford and Sarkar (2000) : 0° approach angle

domes the maximum suction pressures are −0.6 and −0.7, respectively. Figs. 14 and 15 display mean pressure profiles for taps oriented along the *x* direction (centerline) and *z* direction (meridian), respectively. Note that these are not oriented along and cross wind as before.

4.2.3. Ninety degree orientation case

During the 90° flow conditions winds are again symmetric about the two domes, but a stronger recirculation wake region organizes in the gap region, the stagnation region on the downwind dome lifts higher on the dome face, and reduces in magnitude. Fig. 16 compares mean pressure contours measured over the dual domes by Letchford and Sarkar with those calculated by the Fluent

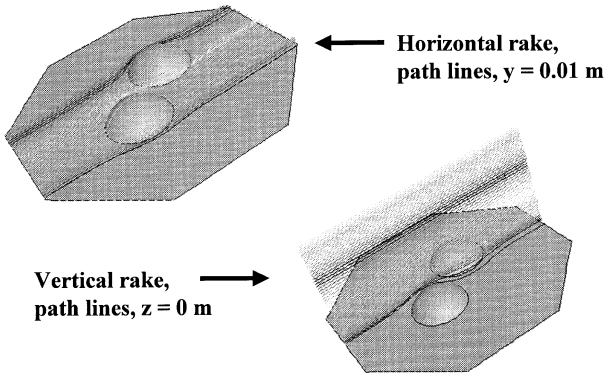

Fig. 13 Path lines over dual hemispherical domes for an octagonal domain and tetrahedral grid elements : 45° approach angle

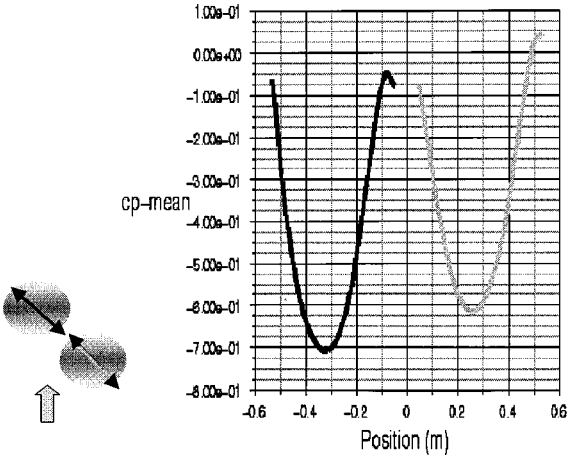

Fig. 14 Centerline mean pressure coefficient profiles over dual hemispherical domes for an octagonal domain and tetrahedral grid elements : 45° approach angle

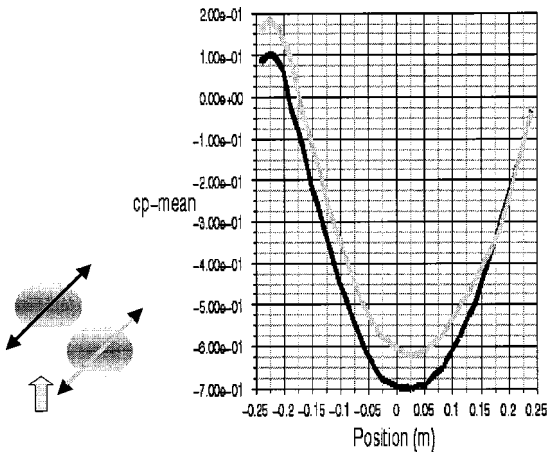

Fig. 15 Meridian mean-pressure coefficient profiles over dual hemispherical domes for an octagonal domain and tetrahedral grid elements : 45° approach angle

programs. The experimental contours display an unexpected asymmetric pattern on the downwind dome, which suggests that the flow may have diverted preferentially to the right (perhaps due to a Coanda like flow attachment behavior or the presence of coal elevators included during the bulk storage dome wind tunnel tests).

Figs. 17 and 18 show comparisons between the up- and downwind dome mean pressure coefficient profiles when the domes are arranged tandem (one behind the other). The centerline pressures for the downwind dome are similar over the forward face although displaced toward the apex, but the maximum suction pressures were reduced due to sheltering from the upwind dome. Meridian pressures on the downwind dome are offset about 0.1 of *Cp* toward higher pressures.

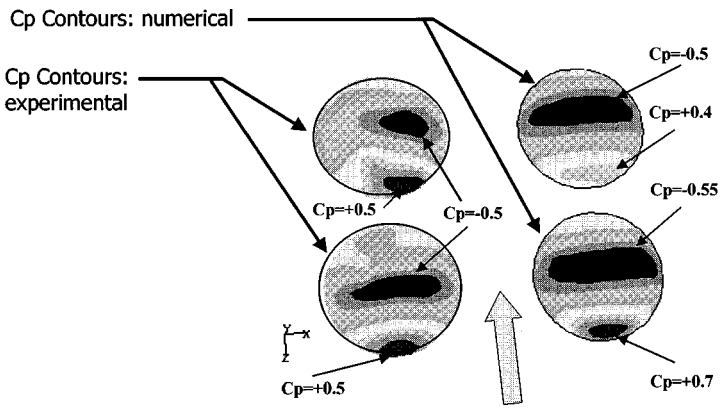

Fig. 16 Contour isopleths of mean-pressure coefficient over dual hemispherical domes for wind-tunnel measurements of Letchford and Sarkar (2000) and numerically calculated cases for octagonal domain and tetrahedral grid elements : 90° approach angle

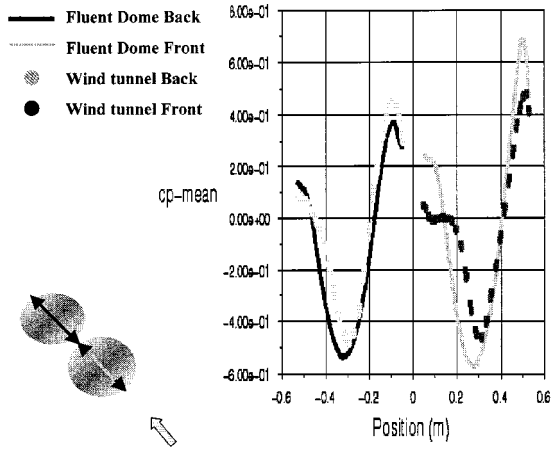

Fig. 17 Centerline mean pressure coefficient profiles over dual hemispherical domes compared to wind-tunnel measurements of Letchford and Sarkar (2000) : 90° approach angle

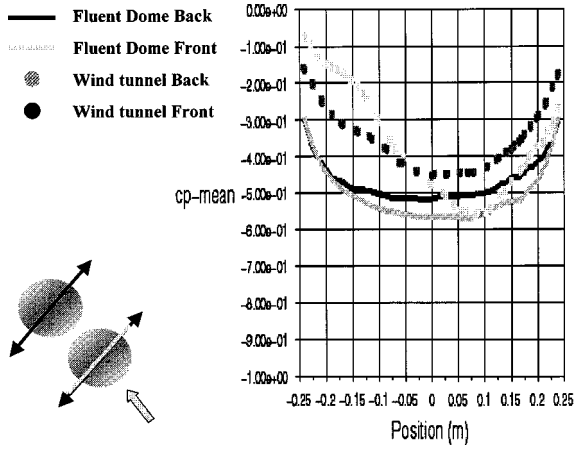

Fig. 18 Meridian mean pressure coefficient profiles over dual hemispherical domes compared to wind-tunnel measurements of Letchford and Sarkar (2000) : 90° approach angle

4.2.4. Dome lift and drag forces

Tables 1 and 2 summarize pressure and viscous drag and lift coefficients for the different single and dual dome configurations, respectively. The drag coefficient, C_D is defined as the force in the windward direction divided by the dynamic head at the dome apex and the projected plan area of the dome, i.e., $F / (1/2\ \rho\ U^2\ A_p)$. The lift coefficient, C_L, is defined as the lift force in the upward direction divided by the dynamic head at the dome apex and the ground plane area of the dome, i.e., $F_L / (1/2\ \rho\ U^2\ A_o)$. Note the significant increase in the dual dome downwind pressure drag compared to the single smooth dome case. On the other hand, the lift forces over the dual domes

Table 1 Drag coefficients for various dome configurations

Dome Configuration	$(C_D)_{\text{Pressure}}$	$(C_D)_{\text{Viscous}}$	$(C_D)_{\text{Total}}$
Single - smooth	0.322	0.023	0.345
Single - rough	0.332	0.063	0.395
Double 0^o - left	0.379	0.025	0.403
Double 0^o - right	0.381	0.025	0.406
Double 45^o - upwind	0.339	0.023	0.361
Double 45^o - downwind	0.328	0.025	0.353
Double 90^o - upwind	0.282	0.035	0.317
Double 90^o - downwind	0.332	0.027	0.356

Table 2 Lift coefficients for various dome configurations

Dome Configuration	$(C_L)_{\text{Pressure}}$	$(C_L)_{\text{Viscous}}$	$(C_L)_{\text{Total}}$
Single - smooth	0.392	0.000	0.392
Single - rough	0.361	0.002	0.363
Double 0^o - left	0.352	0.000	0.352
Double 0^o - right	0.345	0.000	0.345
Double 45^o - upwind	0.257	0.000	0.257
Double 45^o - downwind	0.321	0.000	0.321
Double 90^o - upwind	0.196	0.000	0.196
Double 90^o - downwind	0.240	0.000	0.250

were less than of the isolated dome. Drag and lift values calculated for the wind tunnel experiments were considerably smaller, but are believed to be anomalous due to the deviations previously observed in the pressure coefficient profiles.

5. Conclusions

Mean pressure distributions over domes formed from truncated hemispheres have been calculated for single and paired dome sets. Reynolds effects at conditions studied appear minimal. The three turbulence models specified during calculations produced only minor variations in dome pressure coefficient distributions. Surface roughness is found to reduce mean suctions. Wake effects are found to displace pressure contours and also modify mean suctions.

References

Newman, B.G., Ganguli, Shristave, S.C. (1984), "Flow over spherical inflated buildings", *J. Wind Eng. Ind. Aerod.*, **17**, 305-327.

Maher, F.J. (1965), "Wind loads on basic dome shapes", *J. Struct Div.*, ASCE, ST3 , 219-118.

Taniguchi, S. and Sakamato, H. (1981), "Time averaged aerodynamic forces acting on a hemisphere immersed in a turbulent boundary", *J. Wind Eng. Ind. Aerod.*, **9**, 257-273.

Toy, N., Moss, W.D. and Savory, E. (1983), "Wind tunnel studies on a dome in turbulent boundary layers", *J. Wind Eng. Ind. Aerod.*, **1**, 201-212.

Savory, E. and Toy, N (1986), "Hemispheres and hemisphere-cylinders in turbulent boundary layers", *J. Wind*

Eng. Ind. Aerod., **23**, 345-354.
Ogawa, T., Nakayama, Murayama, S. and Sasaki, Y. (1991), "Characteristics of wind pressures on basic structures with curved surfaces and their response in turbulent flow", *J. Wind Eng. Ind. Aerod.*, **38**, 427-438.
Taylor, T.J. (1991), "Wind pressures on a hemispherical dome", *J. Wind Eng. Ind. Aerod.*,**40**, 199-213.
Letchford, C.W. and Sarkar, P.P. (2000), "Mean and fluctuating wind loads on rough and smooth domes", *Proceedings of BBAA IV Colloquium*, Ruhr-Univ Bochum, Germany, Fall 2000, 19.
Wilcox, D.C. (1993), *Turbulence Modeling for CFD*, DCW Industries, La Canada, CA, 450.
Spalart, P.R. and Allmaras, S.R. (1992), "A one-equation turbulence model for aerodynamic flows", American Institute of Aerodynamics and Astronautics, Paper 92-439, Reno, Nevada.